Brain Imaging and Behavior (2009) 3:154–166
DOI 10.1007/s11682-008-9057-9

Characterization of Atrophic Changes in the Cerebral Cortex Using Fractal Dimensional Analysis

Richard D. King · Anuh T. George · Tina Jeon · Linda S. Hynan · Teddy S. Youn · David N. Kennedy · Bradford Dickerson · and the Alzheimer's Disease Neuroimaging Initiative

Received: 7 August 2008 / Accepted: 18 December 2008 / Published online: 25 January 2009

Abstract The purpose of this project is to apply a modified fractal analysis technique to high-resolution T1 weighted magnetic resonance images in order to quantify the alterations in the shape of the cerebral cortex that occur in patients with Alzheimer's disease. Images were selected from the Alzheimer's Disease Neuroimaging Initiative database (Control N=15, Mild-Moderate AD N=15). The images were segmented using a semi-automated analysis program. Four coronal and three axial profiles of the cerebral cortical ribbon were created. The fractal dimensions (D_f) of the cortical ribbons were then computed using a box-counting algorithm. The mean D_f of the cortical ribbons from AD patients were lower than age-matched controls on six of seven profiles. The fractal measure has regional variability which reflects local differences in brain structure. Fractal dimension is complementary to volumetric measures and may assist in identifying disease state or disease progression.

Keywords Fractal dimension · Alzheimer's disease · Neuroimaging initiative · Cerebral cortex · Fractal analysis

Data used in the preparation of this article were obtained from the Alzheimer's Disease Neuroimaging Initiative (ADNI) database (www.loni.ucla.edu/ADNI). As such, the investigators within the ADNI contributed to the design and implementation of ADNI and/or provided data but did not participate in the analysis or writing of this report.

R. D. King (✉) · A. T. George · T. Jeon · T. S. Youn
Department of Neurology,
University of Texas Southwestern Medical Center,
5323 Harry Hines Blvd,
Dallas, TX 75390-9129, USA
e-mail: richardD.king@utsouthwestern.edu

R. D. King · A. T. George · T. Jeon
Center for BrainHealth, University of Texas at Dallas,
Dallas, TX, USA

L. S. Hynan
Department of Clinical Sciences, Division of Biostatistics,
University of Texas Southwestern Medical Center,
Dallas, TX, USA

L. S. Hynan
Department of Psychiatry,
University of Texas Southwestern Medical Center,
Dallas, TX, USA

D. N. Kennedy
Center for Morphometric Analysis, Massachusetts General Hospital,
Harvard Medical School,
Boston, MA, USA

B. Dickerson
Department of Neurology, Massachusetts General Hospital,
Harvard Medical School,
Boston, MA, USA

Introduction

In the last decade, quantitative volumetric MRI studies of regional human neuroanatomy *in vivo* have contributed greatly to knowledge of macroscopic anatomical changes associated with aging, neurological disease, and psychiatric disease (Toga and Thompson 2002). Currently there exist several techniques for assessment of cerebral morphology, such as manual ROI-based volumetric approaches (Jack et al. 2005), hippocampal shape analysis (Csernansky et al. 2005b), voxel-based morphometry (Ashburner and Friston 2000; Good et al. 2001), cortical pattern matching (Thompson et al. 1998, 2001), brain boundary shift integral (Fox et al. 2000), cortical thickness (Fischl and Dale 2000; Fjell et al. 2006; Walhovd et al. 2005), and regional cortical segmentation (Rademacher et al. 1993). These techniques can reliably differentiate patients with Alzheimer's disease (AD) from controls by demonstrating decreases in brain

volumes (Csernansky et al. 2005a; Dickerson et al. 2005; Dickerson and Sperling 2005; Du et al. 2007; Jack et al. 1999; Killiany et al. 2000; Korf et al. 2004; Visser et al. 1999; Wang et al. 2003). Volumetric characterization is one of many aspects of human anatomical structure. Additional information not available by volumetric analysis may be gained using other analysis techniques, such as shape analysis (Guido et al. 2001).

Shape characterization can be a useful method for identifying clinically relevant information on neuroimaging scans (Casanova et al. 1990; Csernansky et al. 2005b; Wang et al. 2003). One method, which is receiving increasing usage in recent years, is to characterize the shape complexity of the brain using a measure known as fractal dimension. Fractal dimension analysis was first made popular by a series of works by Benoit Mandelbrot in the late 1970s and early 1980s (Mandelbrot 1977, 1982). These analytic techniques can capture very complicated structures using relatively simple computational algorithms. Scientists have used fractal analysis for many years to quantify geologic phenomena such as decay of coastlines, analyzing cracks in crystal structure, botanical simulation, and atmospheric modeling (Herbert and Croft 1996). It has been proposed that these same principles could be used to quantify the spatial properties of the surface of the brain.

Studies using anatomical data from either gross specimens (Hofman 1991) or magnetic resonance images (Cook et al. 1995; Kiselev et al. 2003; Lee et al. 2004; Majumdar and Prasad 1988) have demonstrated that the human cerebral cortex exhibits fractal properties, such as being statistically self-similar (magnification of smaller scale structure resembles the large scale structure). The underlying cerebral white matter, as well as the cerebellum and supporting white matter tracts are also amenable to study using fractal approaches (Esteban et al. 2007; Liu et al. 2003; Zhang et al. 2006, 2007).

The fractal properties of the cerebral cortex arise secondary to folding (Hofman 1991). There are numerous methods for quantifying the degree of folding of the cortex, such as computing the gyrification index (GI), which compares the ratio of the total brain surface to the superficially exposed brain surface (Moorhead et al. 2006; Zilles et al. 1988, 1989). An analogous method is the computation of folding area, which is the ratio of the area of cortex located within folded regions to the total surface area. Im et al. (2006) demonstrated that changes in folding area, as well as sulcal depth and cortical thickness, have significant effects on the fractal dimension of the cortex in normal adults.

This study builds upon previous fractal imaging studies of clinical patient populations in two important ways. First, the anatomical structure of interest is the entire cortical ribbon rather than just the inner or outer surface. Most of the previous studies examining the clinical uses of fractal analysis of the cortex have focused on the cortical boundaries (either the pial surface or the grey/white junction, but not both). When fractal dimension is calculated on pial surfaces, the value is negatively correlated cortical thickness, but positively correlated with folding area and curvature (Im et al. 2006; Jiang et al. 2008). Thus, a degenerative process that caused cortical thinning and widening of sulci (decreased folding area) would have counteracting effects on the measured fractal dimension. We hypothesize that these counteracting effects will instead be complementary when cortical thickness is directly incorporated into the fractal dimension calculation.

Second, this approach is applied to Alzheimer's disease. Given that the fractal properties of the cortex arise secondary to gyrification, diseases that alter gyrification become a natural target for fractal analysis. In Alzheimer's disease, the loss of neurons and subsequent axonal degeneration leads to cerebral atrophy; the effects on the cerebral cortex are widening of sulci and thinning of the cortical ribbon (Thompson et al. 2007). Although it is probable that AD alters cortical gyrification, this has not yet been formally studied. We therefore hypothesize that the fractal dimension of the cortical ribbon of patients with Alzheimer's disease will be significantly lower than age-matched controls with normal cognition. We also hypothesize that there will be regional variation in these findings as there are known regional variations in the degree of AD pathology.

Materials and methods

The data used in this article were obtained from the Alzheimer's Disease Neuroimaging Initiative (ADNI) database (www.loni.ucla.edu/ADNI). The ADNI project was launched in 2003 by the National Institute on Aging (NIA), the National Institute of Biomedical Imaging and Bioengineering (NIBIB), the Food and Drug Administration (FDA), by private pharmaceutical companies, and by non-profit organizations, as a $60 million, 5-year public–private partnership. The primary goal of ADNI has been to test whether serial magnetic resonance imaging (MRI), positron emission tomography (PET), other biological markers, and clinical and neuropsychological assessment can be combined to measure the progression of mild cognitive impairment (MCI) and early Alzheimer's disease (AD). ADNI is the result of the efforts of many co-investigators from a broad range of academic institutions and private corporations, and subjects have been recruited from over 50 sites across the U.S. and Canada. Determination of sensitive and specific markers of very early AD progression is intended to aid researchers and clinicians in developing

new treatments and monitor their effectiveness, as well as lessen the time and cost of clinical trials. For up-to-date information see www.adni-info.org.

Subjects were selected randomly from within a clinical database category (i.e. control, mild Alzheimer's disease). Each patient in the study has had a standardized baseline clinical evaluation as detailed elsewhere (Weiner MW. Alzheimer's Disease Neuroimaging Initiative: Grant application [online]. Available at: www.loni.ucla.edu/ADNI/PDF/Grant.pdf). This study focused primarily on Mini Mental Status Exam (MMSE) and Clinical Dementia Rating (CDR) scores. For the CDR score, a rating of 0 indicates normal cognition, 0.5 indicates questionable or very mild dementia, 1 indicates mild dementia, 2 indicates moderate dementia, and 3 indicates severe dementia (Morris 1997). The MMSE has a scoring of 30 points, with higher scores indicating better performance (Folstein et al. 1975).

Shortly after the baseline visit, all subjects underwent a 1.5 T MRI scan. In addition, 25% of the subjects in each cohort underwent a 3 T MRI. Patients returned for follow-up visits at 3, 6, and 12 months. The longitudinal plan includes repeat imaging at 24 and 36 months (Mueller et al. 2005). The image sequence of choice for obtaining anatomical data was the MP RAGE sequence (magnetization-prepared 180° radio-frequency pulses and rapid gradient-echo). The parameters are: axial orientation, 6.4 ms TR, 4.4 ms TE, 12° FA, 49.9 kHz BW (195 Hz/px), 24× 19.2 cm FOV, 256×192 matrix, 124 contiguous partitions, each 1.2 mm in thickness. The inversion time (TI) and the delay time (TD) are 1,000 and 500 ms respectively. The MP RAGE-based images of 15 patients with varying degrees of clinically diagnosed Alzheimer's disease, as well as images from 15 age and gender matched controls, were selected from the online database www.loni.ucla.edu/ADNI.

Segmentation procedure

The cortical ribbons used in this paper were generated from the MR images using a software suite called *FreeSurfer*. The technical details of these procedures are described in prior publications (Dale et al. 1999; Fischl et al. 1999, 2002, 2004; Han et al. 2006; Yu et al. 2007). *FreeSurfer* contains a set of tools for analysis and visualization of structural and functional brain imaging data. The program includes tools for anatomical analyses and labeling of cortical and subcortical regions.

Processing the images occurred in several steps automatically through the *FreeSurfer* suite. The original images were converted from the DICOM format into a single file with all images from a particular scan protocol. Following motion correction and intensity normalization, extracerebral voxels were removed, using a "skull-stripping" procedure. Head position was normalized along the commissural axis, and then cortical regions were labeled using an automated procedure. A preliminary segmentation of the grey matter from the white matter was generated based on intensity differences and geometric structure differences in the grey/white junction (Fischl and Dale 2000). The pial surface was generated using outward deformation of the grey/white surface with a second-order smoothness constraint. The smoothness constraint allowed the pial surface to be extended into otherwise ambiguous areas. The resulting surface has sub-millimeter accuracy (Dale et al. 1999; Fischl and Dale 2000).

Slice selection

Two dimensional images for analysis were selected from four locations in the coronal plane and three locations in the axial plane. These locations were selected because they were easy to reliably identify, and because the sections intersect areas known to be involved in pathological studies of brains from patients with Alzheimer's disease. For example, the anterior hippocampus can be well visualized on a coronal section through the level of the mammillary bodies (Salamon et al. 2005). In the coronal plane, slices were taken through the most anterior tip of the temporal lobe (Coronal 1), the mammillary bodies (Coronal 2), the superior colliculus (Coronal 3), and the most posterior edge of the corpus callosum (Coronal 4). In the axial plane, the slices intersect the inferior colliculus (Axial 1), the massa intermedia of the thalamus (Axial 2), and the superior margin of the corpus callosum (Axial 3). In Fig. 1, these locations are demonstrated on a skull-stripped midline saggital brain image, along with sample ribbons from a control subject and a patient with moderate Alzheimer's disease.

Note that the cortical ribbon seen in the 2D slices in most cases will overestimate the true cortical thickness. The actual thickness of the cortex can only be accurately computed when the plane of the sectioning is orthogonal to the cortical surface. As such, the cortical ribbon profile will be idiosyncratic to the angle and plane of sectioning. However, as long as the angle and plane of sectioning are selected in a consistent manner, the resulting fractal complexity measure can still be used to compare between patients as well as between scans on the same patient. It was necessary to perform the 2D slicing and image analysis in the original image space since spatial transformations (e.g. Tailarach transformation) would alter the value of the fractal measurements.

The ability of a rater to consistently select slices (intra-rater reliability) was determined by having a rater (RDK) perform the slice selection twice on eight subjects. The Intra-class Correlation Coefficient (ICC) for slice number

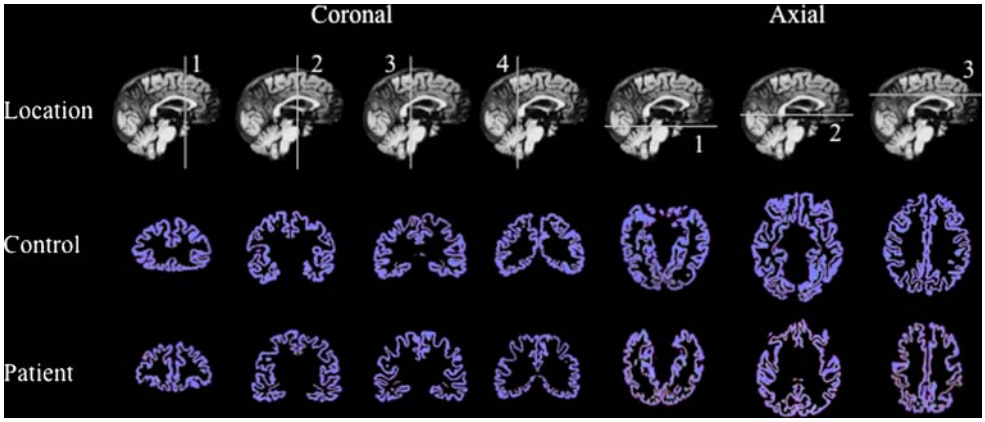

Fig. 1 Example of two-dimensional cortical ribbons from a control subject and a patient with Alzheimer's disease taken from seven locations. Cortical ribbons from seven sectioning planes (four coronal and three axial) were selected for fractal analysis. The locations and orientations of these planes are described in the text. The *first row* identifies these planes as *solid white lines* on a mid-line saggital image. Non-cortical structures (cerebellum, white matter, deep grey matter, and brain stem) were not included in the fractal analysis of the cerebral cortex, but are displayed for spatial reference purposes. The *second row* displays the cortical ribbon extracted from a control patient with normal cognition (CDR=0). In the *third row*, the cortical ribbons from the same locations are shown for a patient with moderate Alzheimer's disease (CDR=2). Note the thinner cortical ribbon and widened sulci in the patient compared to the control subject

was 0.9973 (Model 2, Individual). The ICC for the fractal dimension analysis was 0.6128 (Model 2, Individual). To test the reliability between raters, three trained experts (RDK, ATG, TJ) each selected 30 slice locations from blinded patient data. The ICC was 0.9992 (Model 2, Meaned).

Creating the cortical ribbons

The two-dimensional projections of the pial and grey/white boundaries created through *FreeSurfer* were saved and converted to a standard graphic image format (Targa Graphics, or.tga). Discontinuities in the graphic images were filled in manually, and non-cortical pixels were removed. A profile of the 2D cortical ribbon was created by filling in the enclosed area between the two boundaries. 2D images of the pial boundary and grey/white boundary were then saved as a black and white graphic file, which could be read by the fractal analysis software. See Fig. 2 for a graphic representation of this procedure.

Computing the fractal dimension of the cortical ribbons

There are several approaches for computing the fractal dimension of objects, such as caliper methods (Mandelbrot 1982; Smith et al. 1989; Takayasu 1990), box-counting algorithms (Caserta et al. 1995; Mandelbrot 1982), dilation methods (Fernandez and Jelinek 2001), and spatial frequency analysis (Kiselev et al. 2003). We selected a box-counting algorithm because of the simplicity of implementation as well as for comparison to other studies that use this method to examine fractal properties of the human brain (Cook et al. 1995; Esteban et al. 2007; Im et al. 2006; Lee et al. 2004; Liu et al. 2003; Majumdar and Prasad 1988; Zhang et al. 2006, 2007). The algorithm counts the number of boxes needed to cover the ribbon at a given box scale. The scale is changed, and the process is repeated. The fractal dimension of an object, also known as the Hausdorf–Besikovich dimension, is computed as the ratio of the change in the log of the box count to the change in the log of the box size (see Eq. 1).

$$D_{\mathrm{f}} = -\frac{\Delta \log(\text{box count})}{\Delta \log(\text{box size})} \tag{1}$$

The box-counting algorithm for this project was implemented using a freeware program called *Fractal Dimension Calculator*, or *FDC* (Bourke, http://local.wasp.uwa.edu.au/~pbourke/fractals/fracdim/). *FDC* provides visual tracking for confirmation of proper box-tiling, and provides results as a text file. The raw data for box count and box size were imported into Excel (Microsoft, Seattle WA) for range determination and statistical analysis. Several steps were taken to minimize known limitations of the box-counting method. For each box size, the tiling was repeated 100 times with random offsets in initial box location in order to find the minimum box count required to cover the image (i.e. the best fit). This reduces errors from geometrical placement of the counting boxes. Because fractal objects in nature have a limited spatial range over which they have fractal properties, we only computed the fractal dimension using data points on the linear portions of the box-count–box-size curve. These are the data points that show scale invariance (i.e. the slope between these points measure at different scale is similar). Linearity was defined as a change in slope between data

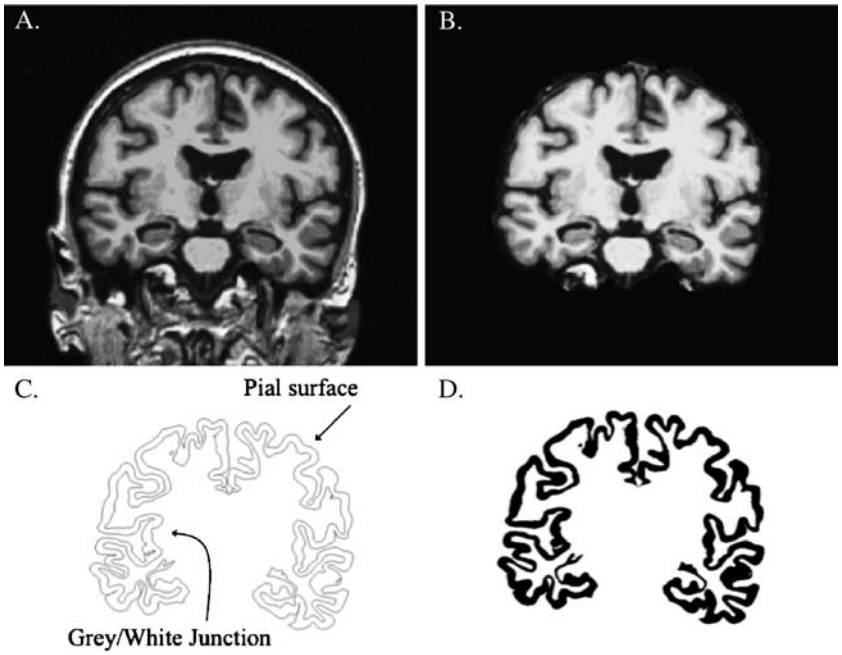

Fig. 2 Magnetic resonance image segmentation and cortical ribbon generation. This figure shows some of the key steps involved in generating a two-dimensional projection of the ribbon of cerebral cortex. Please see the text for full details. **a** This panel shows original magnetic resonance image generated using the MP-RAGE (T1 weighted) sequence. This coronal slice was taken through the mammillary bodies. **b** This is the image after intensity normalization, skull-stripping, and removal of brain stem. **c** The grey/white surface is generated using intensity differences between the grey and white matter on the normalized image. The pial surface was generated using outward deformation of the grey/white surface. **d** The space between the two surfaces in panel C is filled to create the cortical ribbon

segments of less than 0.1. The fractal dimension was then computed using linear regression of the selected points. The resulting regression lines had a coefficient of determination (R^2)>0.999, and a standard deviation less than 0.04. A graphical representation of this process is shown in Fig. 3.

Determining how cortical thickness and cortical gyrification affect fractal dimensionality

To evaluate effects of changes in gyrification index or cortical thickness on the two dimensional cortical ribbon, we generated artificial data based on a coronal slice from one of the control subjects. For cortical thickness assessment, the cortical ribbon was edited to be of uniform thickness, which was varied from 0.5 to 5 mm. The gyrification pattern was manually edited to either add or remove gyri from the original cortical ribbon. The two modifications were also done simultaneously to look at additive effects.

Comparison with other structural analysis techniques

It is expected that by using a fractal approach (in combination with other approaches), there will be more variance accounted for in the data, and that the ability to correctly classify patients into risk groups will be improved. To determine how the 2D fractal analysis technique compared with other structural approaches, we compared the group separation of the 2D cortical ribbons using fractal analysis to analysis of the normalized 2D cortical ribbon area, the whole-brain volume as a percent of intracranial volume (ICV), and hippocampal volume fraction (% ICV) of all the subjects in his study. The area of the 2D cortical ribbons was computed by counting the number of pixels in the image. The 2D areas were normalized for head size by dividing the area by the anterior–posterior diameter of the skull in the midline at the level of the inferior colliculus. Whole-brain volume fraction was computed by comparing the ratio of the Segmented Brain Volume to the Estimated Intracranial Volume, both of which were measured by *FreeSurfer* during the segmentation process. Hippocampal volumes (right and left) were also measured by *FreeSurfer*. Note that the hippocampus itself was considered a subcortical structure, and was therefore excluded from the cortical ribbons.

Statistical analysis

For the dichotomous measure (gender), the number and percent are provided and χ^2 or Fisher's exact tests, as appropriate, were performed to compare the two groups. For the continuous measures (age and total MMSE score),

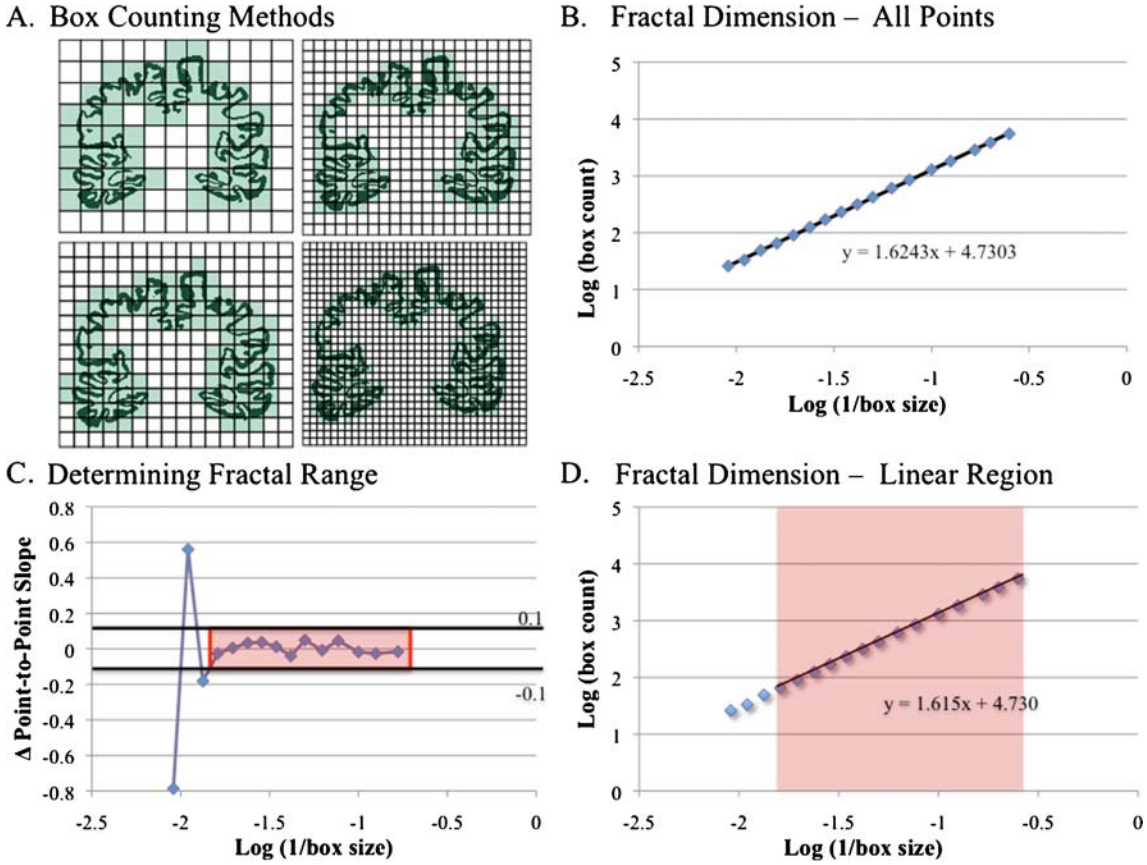

Fig. 3 Computing fractal dimension using a box-counting algorithm. **a** An object is tiled with boxes of a given size, and the number of boxes needed to cover the object is counted. The box size is changed, and the process is repeated. Four examples of tiling are shown in this panel. **b** The fractal dimension of an object is computed by determining the ratio of the change in box count to the change in box size (in log–log space). The least squares regression for all data points is indicated by the *solid line*. **c** To determine the spatial range over which the image shows scale invariance, the change in point-to-point slope is plotted. Those point-pairs with slopes less than the threshold (±0.1) are *highlighted in pink*. **d** The data from panel (**b**) are shown, but the *regression line* is taken only through the linear portion

the mean and standard deviation are provided, and a *t*-test was performed for age. A multivariate analysis of covariance (MANCOVA) was performed on the seven regions comparing groups and using the covariates age and gender; the covariates in all analyses were non-significant and *t*-tests were used to compare the two groups. All statistical tests were checked for violations of assumptions. SPSS V14.0 was used for these analyses. Statistical tests were performed using two sided tests, and $p<0.05$. Effect sizes (Cohen's *d* value) of the three morphometric techniques (fractal analysis, whole-brain volume fraction, and 2D cross-sectional area) were computed using Excel 2003 SP3. A large effect size is indicated by $d>0.8$.

Results

Natural objects display fractal properties (i.e. scale invariance) over a limited spatial range. For the two-dimensional cortical ribbons used in this project, the lower end of the fractal size range was ~3 mm. This was constrained by the spatial resolution of the pixelized image files. The upper end of the fractal size range varied between 26 and 44 mm.

The effect of changing the cortical thickness and/or the gyrification index on the calculated fractal dimension of an artificial cortical ribbon is shown in Fig. 4. When incorporated directly in the fractal analysis, increasing the thickness of the cortical ribbon raises the measured fractal dimension. Increasing the gyrification index has a similar effect. The effect of increasing both GI and cortical thickness simultaneously is a nonlinear addition that further increases dimensionality. For example, the cortical ribbon with the highest dimensionality in Fig. 4 also has the highest gyrification index and highest cortical thickness.

The results of the fractal analysis of the two-dimensional cortical ribbons (four coronal slices and three axial slices) from control subjects and patients with mild to moderate Alzheimer's disease are summarized in Table 1. The table shows the ADNI ID, gender, age, Clinical Dementia Rating (CDR) score, Mini Mental Status Exam (MMSE) score, and

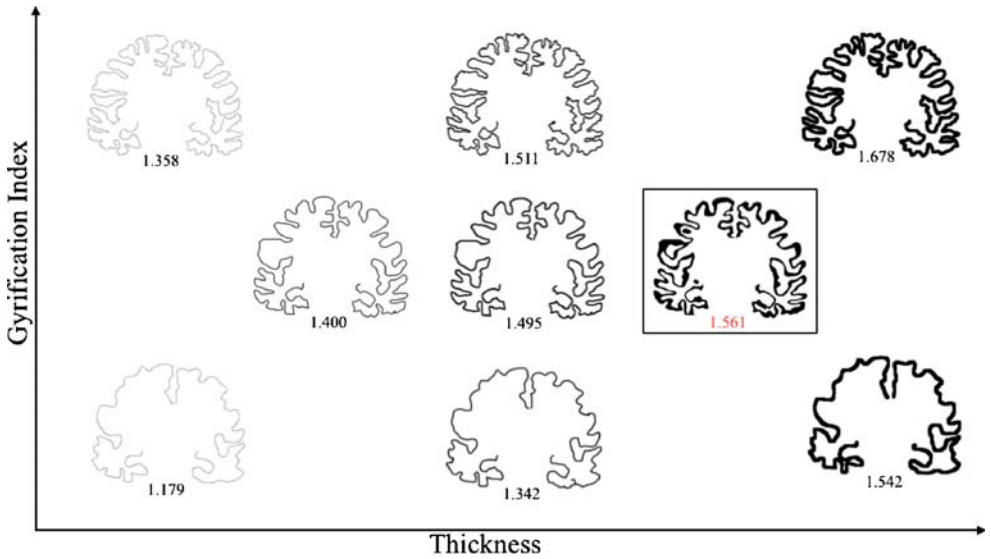

Fig. 4 The effects of cortical thickness and gyrification index on measured fractal dimensionality. A coronal slice from a control subject and its fractal dimension is seen in the box. The remaining cortical ribbons are artificial data demonstrating fractal dimension changes with variation in cortical thickness, gyrification index, and the combination of the two. The fractal dimension of each slice is indicated by the number below the slice. Changes in cortical thickness are seen on the horizontal axis with increasing thickness towards the right. Changes in the gyrification index are seen on the vertical axis with values increasing upwards. Thinning of the cortical ribbon and lowering the gyrification index both decrease fractal dimensionality

the fractal dimension calculated for the cortical ribbon at each location. There were 15 subjects in the control group (53.3% female) and 15 subjects in the AD patient group (53.3% females). Subjects in both groups were similar in age (p=0.90, Controls 75.7±9.6 versus Patients 76.1±7.8). Multivariate models for the covariate of 'age' were not significant.

The scatter-plot in Fig. 5 shows the scores for all of the controls and patients at each location. The mean value of the fractal dimension was higher for the control subjects than for the patients at all locations. There were significant group differences in the analyses for six of the seven regions. These regions include the most anterior tip of the temporal lobe (Coronal 1), the mammillary bodies (Coronal 2), the superior colliculus (Coronal 3), the most posterior edge of the corpus callosum (Coronal 4), the inferior colliculus (Axial 1), and mid thalamus (Axial 2). Slices through and the superior margin of the corpus callosum (Axial 3) showed a trend toward separation, but the difference was not statistically significant. The statistics are summarized in Table 2.

The results of the comparison between fractal analysis, whole brain volume fraction, and two-dimensional cross-sectional area are shown in Table 3. Whole-brain volume comparison between subject groups yielded a strong effect size (d=1.41, p=0.019). On average, the areas of the cortical ribbons from the control group were larger than those from the patients (d=1.37, p=0.009). Similar to fractal analysis, the normalized cross-sectional area measures demonstrated regional variation in terms of the analysis effect size. There were small to medium effect sizes at the first coronal location and the second axial location, and strong effect sizes at the remaining locations. The normalized hippocampal volume measurements showed a strong separation between these same clinical groups with a very large effect size (d=3.78, p<0.001).

Discussion

2D fractal analysis of the cortical ribbon can discriminate patients with different degrees of cerebral atrophy

The fractal technique used in this project successfully discriminated between the two clinical groups in six of the seven slice locations and orientations tested. The analysis identified regional differences in the fractal measurements, which suggests that this slice approach is sensitive to local intrinsic structural variability. Even though it is unlikely that an entire slice will change in its spatial properties, this fractal technique was able to detect enough changes in many of the selected regions to generate a significant difference between the two patient groups.

The fractal analysis approach used in this paper differed from previous papers in that we analyzed the entire 2D profile of the cortical ribbon rather than just the inner or outer boundaries. This approach allows changes in cortical thickness to be directly incorporated into the

Table 1 Summary of clinical data and computed fractal dimension

Patient	Gender	Age	CDR	MMSE	Fractal dimension						
					Coronal 1	Coronal 2	Coronal 3	Coronal 4	Axial 1	Axial 2	Axial 3
141_S_1094	M	76.1	0	30	1.660	1.626	1.637	1.671	1.677	1.632	1.680
131_S_1301	F	72.2	0	30	1.635	1.576	1.590	1.616	1.616	1.596	1.594
002_S_1261	F	71.2	0	30	1.664	1.629	1.654	1.634	1.699	1.637	1.655
002_S_1280	F	70.8	0	30	1.645	1.640	1.617	1.626	1.647	1.632	1.668
002_S_0413	F	76.9	0	29	1.672	1.654	1.640	1.674	1.677	1.667	1.679
002_S_0295	M	84.9	0	28	1.649	1.622	1.618	1.629	1.622	1.645	1.654
002_S_0559	M	79.4	0	29	1.657	1.594	1.612	1.632	1.662	1.651	1.642
002_S_0685	F	89.7	0	30	1.627	1.606	1.634	1.633	1.641	1.597	1.661
003_S_0907	F	88.7	0	30	1.682	1.617	1.612	1.635	1.642	1.635	1.643
003_S_0931	F	86.2	0	28	1.641	1.599	1.610	1.652	1.632	1.617	1.639
003_S_0981	F	84.4	0	29	1.636	1.606	1.604	1.621	1.652	1.624	1.569
011_S_0016	M	66.6	0	30	1.664	1.622	1.636	1.660	1.707	1.654	1.663
011_S_0022	M	63.3	0	29	1.642	1.595	1.597	1.636	1.684	1.650	1.626
020_S_1288	M	60.0	0	30	1.672	1.647	1.657	1.637	1.664	1.675	1.616
073_S_0089	M	65.1	0	30	1.676	1.652	1.652	1.653	1.719	1.676	1.685
Average		*75.7*			*1.655*	*1.619*	*1.625*	*1.641*	*1.663*	*1.639*	*1.645*
009_S_1354	F	59.0	1	20	1.636	1.585	1.600	1.610	1.684	1.599	1.623
012_S_0689	M	64.2	1	19	1.664	1.623	1.612	1.628	1.625	1.627	1.621
011_S_0053	M	80.2	0.5	23	1.622	1.601	1.594	1.639	1.633	1.609	1.615
011_S_0183	F	72.5	1	21	1.627	1.594	1.604	1.609	1.599	1.621	1.636
002_S_0938	F	82.3	1	23	1.609	1.576	1.584	1.596	1.649	1.640	1.673
002_S_0619	M	77.6	1	22	1.616	1.603	1.579	1.592	1.585	1.633	1.616
011_S_0003	M	81.4	1	20	1.618	1.582	1.601	1.627	1.573	1.607	1.659
005_S_0221	M	68.2	2	17	1.647	1.585	1.599	1.614	1.612	1.596	1.616
012_S_0720	F	78.1	2	20	1.585	1.570	1.566	1.578	1.587	1.612	1.611
002_S_0955	F	78.3	0.5	21	1.588	1.567	1.579	1.604	1.589	1.605	1.611
002_S_1070	M	74.3	0.5	22	1.574	1.532	1.556	1.590	1.593	1.593	1.585
007_S_0316	M	82.0	1	19	1.619	1.611	1.611	1.640	1.638	1.642	1.654
006_S_0653	F	73.9	1	20	1.624	1.581	1.566	1.615	1.601	1.621	1.616
007_S_1339	F	80.7	1	21	1.617	1.568	1.609	1.619	1.680	1.614	1.632
027_S_0404	F	88.9	1	22	1.632	1.671	1.620	1.640	1.693	1.656	1.683
Average		*76.1*			*1.618*	*1.590*	*1.592*	*1.613*	*1.623*	*1.618*	*1.630*

For each patient, the ADNI identification number, gender, age, Clinical Dementia Rating (CDR) score, Mini Mental Status Exam (MMSE) score, and fractal dimension assessment for each location are shown. The average values for each clinical group and slice location are italicized. The subjects were placed into either the control group or Alzheimer's disease group by ADNI investigators based upon clinical criteria (including MMSE and CDR scores)

fractal computation. The importance of the combined effect of gyrification index and cortical thickness was shown in Fig. 4. When measured simultaneously, decreases in either variable lowers the fractal dimensionality (i.e., there is positive correlation for both). This is an important technical difference from previous studies because when measured independently, fractal dimension has a positive correlation with gyrification index, but a negative correlation with cortical thickness (Im et al. 2006). This result suggests that fractal measures of the cortical ribbon behave differently than measures of the pial surface, and that ribbon measurements are more likely to be useful in quantifying changes associated with neurodegenerative disease.

Spatial variability and localization

This paper analyzed seven locations as a proof of concept that there are significant changes in the fractal dimension of the cerebral cortical ribbon with Alzheimer's disease. It is not surprising that distinguishing patients with AD from control patients is more successful in some regions than others given the known patterns of variable cortical involvement. For example, pathological analysis of brains with Alzheimer's demonstrates more prominent pathology in medial temporal and parietal lobes compared to occipital lobes (Arnold et al. 1991).

Localization of changes in shape in this paper is not possible beyond the level of individual slices. Moreover,

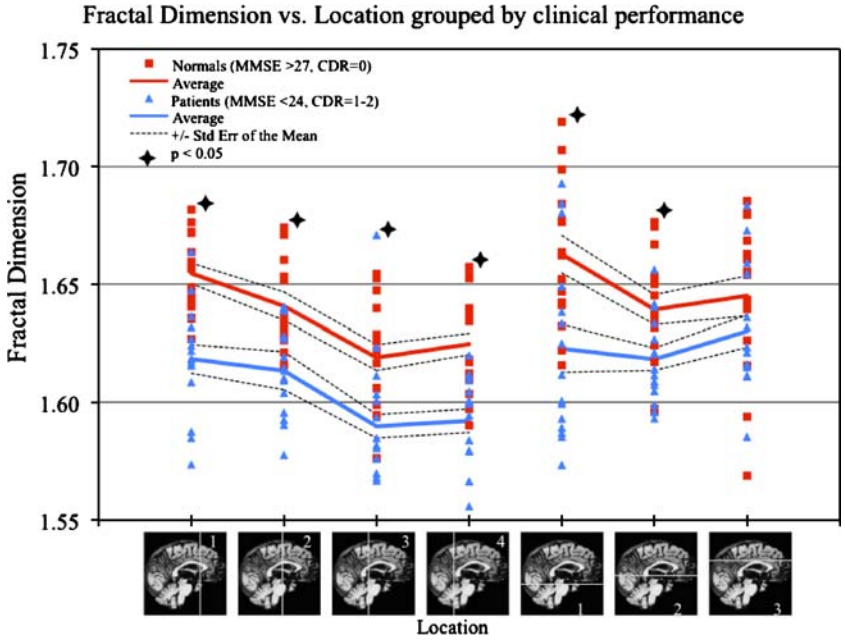

Fig. 5 Fractal dimension scatter-plot for 18 scans of patients in two diagnostic categories. The cortical ribbons for 30 MR scans were analyzed in seven locations described in Fig. 2 using the methods described in Fig. 3 and in the text. For each location, the fractal dimension of the cortical ribbon is plotted for each patient. The *solid lines* indicate the average scores for each performance category. The *dotted lines* indicate ± one standard error of the mean. The subjects are grouped according to clinical category with red squares indicating controls (MMSE scores 28–30) and *blue triangles* indicating the patients (MMSE scores 17–23). The average fractal dimension was higher in all locations for the control group compared to the patient group. The values were statistically significant for all four coronal locations as well as the first two axial locations. See Table 2 for details on the statistical analysis

Table 2 Statistical analysis of fractal dimension data for patients grouped by clinical category

	Baseline group statistics			Fractal dimension statistics								*t* test *p* values
	Normal (*N*=11)	Early AD (*N*=9)	*p* values	Normal (*N*=15)				Early AD (*N*=15)				
				Mean	Std. error	95% confidence Interval		Mean	Std. error	95% confidence interval		
						Lower bound	Upper bound			Lower bound	Upper bound	Group
Age (Mean±SD)	75.7±9.6	76.1±7.7	0.900									
Sex (% F)	53.3%	53.3%	–									
MMSE (Mean±SD)	29.5±0.7	20.7±1.6	–									
Variable												
Coronal 1				1.655	.005	1.644	1.665	1.618	.005	1.608	1.629	<0.001
Coronal 2				1.619	.007	1.604	1.634	1.590	.007	1.575	1.604	0.007
Coronal 3				1.625	.005	1.614	1.635	1.592	.005	1.581	1.603	<0.001
Coronal 4				1.641	.005	1.631	1.650	1.613	.005	1.604	1.623	<0.001
Axial 1				1.663	.009	1.644	1.681	1.623	.009	1.604	1.641	0.004
Axial 2				1.639	.006	1.628	1.651	1.618	.006	1.607	1.630	0.013
Axial 3				1.645	.008	1.629	1.661	1.630	.008	1.614	1.646	0.181

Baseline group statistics: The age differences between the two groups were not statistically significant (computed using two independent samples *t*-test). The two groups were selected to balance gender. The MMSE scores are shown, but were not included in statistical models since this clinical information was part of the initial criteria for categorization. Fractal dimension statistics: All regions were found to have a statistically significant higher mean fractal dimension in the control group except for Axial 3, which showed a trend towards separation. On MANCOVA analysis, neither age nor gender was a statistically significant covariate

Table 3 Statistical comparison of subject category separation using whole-brain volume, fractal dimension, cross-sectional area, or hippocampal volume

Analysis Technique	Location	Mean value		Cohen's *d*	*p* value
		Control	Patient		
Fractal dimension	Coronal 1	1.655	1.618	1.77	<0.001
	Coronal 2	1.619	1.590	1.06	0.007
	Coronal 3	1.625	1.592	1.60	<0.001
	Coronal 4	1.641	1.613	1.49	<0.001
	Axial 1	1.663	1.623	1.13	0.004
	Axial 2	1.639	1.618	0.97	0.013
	Axial 3	1.645	1.630	0.50	0.181
Normalized cross-sectional area	Coronal 1	60.09	55.91	0.47	0.349
	Coronal 2	86.35	79.49	1.26	0.013
	Coronal 3	87.77	78.60	1.34	0.010
	Coronal 4	89.53	83.20	0.78	0.143
	Axial 1	124.78	108.07	1.44	0.012
	Axial 2	127.54	123.61	0.41	0.395
	Axial 3	128.30	115.70	0.94	0.067
Whole brain volume (% ICV)		68.55	61.35	1.41	0.019
R. & L. hippocampal volume (% ICV)		0.481	0.329	3.78	<0.001

Effect size (Cohen's *d*) and significance of the *F* statistic (*p* value) are shown for the mean differences between patient categories for fractal dimension, normalized cross-sectional area, whole brain volume, and hippocampal volume. The whole brain volume and hippocampal volume are normalized by the intracranial volume to account for variation in head size. The locations that showed statistical significance on the fractal dimension test (coronal 1–4 and axial 1–2) had effect sizes of similar magnitude to the whole brain volume measure, and generally larger than cross-sectional area measures. The hippocampal volume measurement had a very large effect size on this subject population

the selected locations may not represent the best or most significant locations. While the locations selected for this study were good candidates, a systematic analysis of many more slices and slice orientations may yield locations and orientations that are more sensitive than the ones used in this study. Localization of regions where the greatest change between groups occurs would also require either considerably more slices or a localized three-dimensional cortical ribbon analysis technique. Both approaches are interesting future directions, but would require a more fully automated method of data analysis and custom software to be practical. This study was not intended to provide detailed localization for anatomical/pathological correlation. That type of analysis could be better performed using a three-dimensional measure that takes into account the entire cortical surface. Such a method is currently under development.

Sources of variability in the fractal measure

Methods for group comparisons in imaging studies usually involve transformation into a common image space. However, such an approach is not possible in this study since the process or transformation dramatically alters the imaging data. The 2D slicing and subsequent fractal analysis are required to be performed in the original image space, and consequently the images will not be exactly co-registered. This is a recognized limitation of the current method, and it unquestionably adds noise to the analysis. Despite this limitation, we were able to identify significant differences between the two groups. It may be possible to dramatically reduce this source of noise by using unbiased diffeomorphic atlases (Joshi et al. 2004) prior to group comparisons.

Another potential source of noise is the observation that the junction between the cerebral cortex and underlying white matter becomes more difficult to discriminate in older subjects. This phenomenon is not likely to impair the validity of the fractal measure for several reasons. First, the MP-RAGE sequence used in the ADNI protocol enhances the grey-white contrast (much greater than what is seen on computed tomography or T1-weighted magnetic resonance images). Second, the image intensities were normalized using FreeSurfer, and image normalization was checked prior to analysis. The accuracy of the FreeSurfer grey/white segmentation has not been shown to be less accurate as a function of age. Additionally, the two groups were age matched, and age was not found to be a statistically significant covariate. Finally, if there were any net effect of ambiguity in the grey/white interface, it would cause some smoothing of the junctional boundary. Rather than confounding the fractal data, this smoothing would become

data. The smoother inner boundary of the cortical ribbon would be one of several variables (including cortical thickness and gyrification index) that are incorporated into the fractal measure.

Using advancing MRI technology to improve the fractal dimension measure

There are several factors that limit the minimum spatial scale for the fractal analysis. These include limitations on the resolution of the initial magnetic resonance image (as determined by scanning parameters and magnetic field strength), limitations on the process of image segmentation (accuracy of pial and grey-white boundaries), and limitation on the resolution of the digitized images used in the fractal analysis software. The MP-RAGE images used in this project, which were obtained using the ADNI protocol on 1.5 T magnets, had a resolution of 1.25 mm×1.25 mm× 1.2 mm. It is now possible to obtain higher resolution data with relatively routine imaging technology (e.g., 800 μm isotropic). These higher resolution images may extend the lower spatial scale of the fractal analysis, and thereby increase the sensitivity of the images to subtle changes in shape. The image segmentation through *FreeSurfer* yields sub-millimeter resolution surfaces, and as such is unlikely to be the limiting factor in this analysis. In this study, the limiting factor was the process of pixelizing the segmented images into the appropriate image format. The best way to overcome this obstacle is to perform the fractal analysis directly on the MRI data, thereby skipping the pixilation process entirely. Development of this custom software is a major focus for future work.

Comparing and combining fractal data with other techniques

Many established techniques, including whole-brain and hippocampal volume measurements, are being applied to the Alzheimer's Disease Neuroimaging Initiative data. When compared to whole brain volume measurements, the effect size of the fractal analysis was equal or greater in six of the seven regions. The differences in hippocampal volume between clinical groups were very robust and had a larger effect size than results derived from fractal analysis. The correlation between hippocampal volumes and cortical fractal dimension were weak, suggesting that the two measures are largely independent. Thus, combining the two measures may improve power of discrimination over either measure independently. It will be of interest to determine how well fractal analysis performs in patients with milder symptoms, in whom it may be valuable to have additional types of measures beyond hippocampal volume.

Using fractal dimension prospectively

The observed variation in local cortical involvement also presents a future opportunity to identify patterns in regional atrophy that correlate with different forms of neurodegenerative disease. This will require comparing systematic sections of patients with differing forms of dementia (i.e., AD, Lewy Body dementia, Fronto-temporal dementia) to identify locations that best separate them from normal patients as well as from each other. The eventual goal of this technique is to develop a classification method that is sensitive and specific for various forms of neurodegenerative disease. The current study was not sufficiently powered to determine the range of "normal". Indeed, the range of normal is likely to be dependent upon not only age but also region. With the development of automated high-throughput systems, it would be possible to evaluate much larger cohorts (i.e. the entire ADNI database). At that point, fractal scores can be compared with population norms (corrected for age) to generate *Z* scores, and the sensitivity and specificity of the fractal values can be determined.

Acknowledgements This project has been funded by generous support from the UNCF*Merck Science Initiative and the Harold Amos Medical Faculty Development Program (a program of the Robert Wood Johnson Foundation), NIH grant NS34189, and by NIA grant 5P30AG012300. In addition, the authors would like to thank Dr. John Hart for his helpful comments and overall tremendous support of this project. We also thank Paul Bourke, Dr. Mike Kraut, Ms. Sharon O'Meara, and the staff at the Center for BrainHealth at the University of Texas at Dallas for providing support and infrastructure for this work to proceed. Many thanks are also given to Dr. Roger Rosenberg and the faculty and staff of the Alzheimer's Disease Center at the University of Texas Southwestern Medical Center for providing a forum to discuss ideas developed in this paper. We also thank Dr. Verne Caviness and the members of the Center for Morphometric Analysis at Massachusetts General Hospital for support in learning *FreeSurfer* and technical assistance with the project in general. Data collection and sharing for this project was funded by the Alzheimer's Disease Neuroimaging Initiative (ADNI; Principal Investigator: Michael Weiner; NIH grant U01 AG024904). ADNI is funded by the National Institute on Aging, the National Institute of Biomedical Imaging and Bioengineering (NIBIB), and through generous contributions from the following: Pfizer Inc., Wyeth Research, Bristol-Myers Squibb, Eli Lilly and Company, GlaxoSmithKline, Merck & Co. Inc., AstraZeneca AB, Novartis Pharmaceuticals Corporation, Alzheimer's Association, Eisai Global Clinical Development, Elan Corporation plc, Forest Laboratories, and the Institute for the Study of Aging, with participation from the U.S. Food and Drug Administration. Industry partnerships are coordinated through the Foundation for the National Institutes of Health.

References

Arnold, S. E., Hyman, B. T., Flory, J., Damasio, A. R., & Van Hoesen, G. W. (1991). The topographical and neuroanatomical distribution of neurofibrillary tangles and neuritic plaques in the cerebral cortex of patients with Alzheimer's disease. *Cerebral Cortex (New York, N.Y.)*, *1*(1), 103–116. doi:10.1093/cercor/1.1.103.

Ashburner, J., & Friston, K. J. (2000). Voxel-based morphometry—The methods. *NeuroImage*, *11*(6 Pt 1), 805–821. doi:10.1006/nimg.2000.0582.

Casanova, M. F., Goldberg, T. E., Suddath, R. L., Daniel, D. G., Rawlings, R., Lloyd, D. G., et al. (1990). Quantitative shape analysis of the temporal and prefrontal lobes of schizophrenic patients: A magnetic resonance image study. *The Journal of Neuropsychiatry and Clinical Neurosciences*, *2*(4), 363–372.

Caserta, F., Eldred, W. D., Fernandez, E., Hausman, R. E., Stanford, L. R., Bulderev, S. V., et al. (1995). Determination of fractal dimension of physiologically characterized neurons in two and three dimensions. *Journal of Neuroscience Methods*, *56*(2), 133–144. doi:10.1016/0165-0270(94)00115-W.

Cook, M. J., Free, S. L., Manford, M. R., Fish, D. R., Shorvon, S. D., & Stevens, J. M. (1995). Fractal description of cerebral cortical patterns in frontal lobe epilepsy. *European Neurology*, *35*(6), 327–335. doi:10.1159/000117155.

Csernansky, J. G., Wang, L., Miller, J. P., Galvin, J. E., & Morris, J. C. (2005a). Neuroanatomical predictors of response to donepezil therapy in patients with dementia. *Archives of Neurology*, *62*(11), 1718–1722. doi:10.1001/archneur.62.11.1718.

Csernansky, J. G., Wang, L., Swank, J., Miller, J. P., Gado, M., McKeel, D., et al. (2005b). Preclinical detection of Alzheimer's disease: Hippocampal shape and volume predict dementia onset in the elderly. *NeuroImage*, *25*(3), 783–792. doi:10.1016/j.neuroimage.2004.12.036.

Dale, A. M., Fischl, B., & Sereno, M. I. (1999). Cortical surface-based analysis. I. Segmentation and surface reconstruction. *NeuroImage*, *9*(2), 179–194. doi:10.1006/nimg.1998.0395.

Dickerson, B. C., & Sperling, R. A. (2005). Neuroimaging biomarkers for clinical trials of disease-modifying therapies in Alzheimer's disease. *Neurorx*, *2*(2), 348–360. doi:10.1602/neurorx.2.2.348.

Dickerson, B. C., Salat, D. H., Greve, D. N., Chua, E. F., Rand-Giovannetti, E., Rentz, D. M., et al. (2005). Increased hippocampal activation in mild cognitive impairment compared to normal aging and AD. *Neurology*, *65*(3), 404–411. doi:10.1212/01.wnl.0000171450.97464.49.

Du, A. T., Schuff, N., Kramer, J. H., Rosen, H. J., Gorno-Tempini, M. L., Rankin, K., et al. (2007). Different regional patterns of cortical thinning in Alzheimer's disease and frontotemporal dementia. *Brain*, *130*(Pt 4), 1159–1166. doi:10.1093/brain/awm016.

Esteban, F. J., Sepulcre, J., de Mendizabal, N. V., Goni, J., Navas, J., de Miras, J. R., et al. (2007). Fractal dimension and white matter changes in multiple sclerosis. *NeuroImage*, *36*(3), 543–549. doi:10.1016/j.neuroimage.2007.03.057.

Fernandez, E., & Jelinek, H. F. (2001). Use of fractal theory in neuroscience: Methods, advantages, and potential problems. *Methods (San Diego, Calif.)*, *24*(4), 309–321. doi:10.1006/meth.2001.1201.

Fischl, B., & Dale, A. M. (2000). Measuring the thickness of the human cerebral cortex from magnetic resonance images. *Proceedings of the National Academy of Sciences of the United States of America*, *97*(20), 11050–11055. doi:10.1073/pnas.200033797.

Fischl, B., Sereno, M. I., & Dale, A. M. (1999). Cortical surface-based analysis. II: Inflation, flattening, and a surface-based coordinate system. *NeuroImage*, *9*(2), 195–207. doi:10.1006/nimg.1998.0396.

Fischl, B., Salat, D. H., Busa, E., Albert, M., Dieterich, M., Haselgrove, C., et al. (2002). Whole brain segmentation: Automated labeling of neuroanatomical structures in the human brain. *Neuron*, *33*(3), 341–355. doi:10.1016/S0896-6273(02)00569-X.

Fischl, B., van der Kouwe, A., Destrieux, C., Halgren, E., Segonne, F., Salat, D. H., et al. (2004). Automatically parcellating the human cerebral cortex. *Cerebral Cortex (New York, N.Y.)*, *14*(1), 11–22. doi:10.1093/cercor/bhg087.

Fjell, A. M., Walhovd, K. B., Reinvang, I., Lundervold, A., Salat, D., Quinn, B. T., et al. (2006). Selective increase of cortical thickness in high-performing elderly—structural indices of optimal cognitive aging. *Neuroimage*, *29*(3), 984–994.

Folstein, M. F., Folstein, S. E., & McHugh, P. R. (1975). "Mini-mental state". A practical method for grading the cognitive state of patients for the clinician. *Journal of Psychiatric Research*, *12*(3), 189–198. doi:10.1016/0022-3956(75)90026-6.

Fox, N. C., Cousens, S., Scahill, R., Harvey, R. J., & Rossor, M. N. (2000). Using serial registered brain magnetic resonance imaging to measure disease progression in Alzheimer disease: Power calculations and estimates of sample size to detect treatment effects. *Archives of Neurology*, *57*(3), 339–344. doi:10.1001/archneur.57.3.339.

Good, C. D., Johnsrude, I. S., Ashburner, J., Henson, R. N., Friston, K. J., & Frackowiak, R. S. (2001). A voxel-based morphometric study of ageing in 465 normal adult human brains. *NeuroImage*, *14*(1 Pt 1), 21–36. doi:10.1006/nimg.2001.0786.

Guido, G., Styner, M., Shenton, M. E., & Leiberman, J. A. (2001). Shape versus size: Improved understanding of the morphology of brain structures. *Lecture Notes in Computer Science*, *2208*, 24–32.

Han, X., Jovicich, J., Salat, D., van der Kouwe, A., Quinn, B., Czanner, S., et al. (2006). Reliability of MRI-derived measurements of human cerebral cortical thickness: The effects of field strength, scanner upgrade and manufacturer. *NeuroImage*, *32*(1), 180–194. doi:10.1016/j.neuroimage.2006.02.051.

Herbert, D. E., & Croft, P. (1996). *Chaos and the changing nature of science and medicine: An introduction: Mobile, AL, April 1995*. Woodbury, N.Y.: AIP.

Hofman, M. A. (1991). The fractal geometry of convoluted brains. *Journal fur Hirnforschung*, *32*(1), 103–111.

Im, K., Lee, J. M., Yoon, U., Shin, Y. W., Hong, S. B., Kim, I. Y., et al. (2006). Fractal dimension in human cortical surface: Multiple regression analysis with cortical thickness, sulcal depth, and folding area. *Human Brain Mapping*, *27*(12), 994–1003. doi:10.1002/hbm.20238.

Jack, C. R. Jr., Petersen, R. C., Xu, Y. C., O'Brien, P. C., Smith, G. E., Ivnik, R. J., et al. (1999). Prediction of AD with MRI-based hippocampal volume in mild cognitive impairment. *Neurology*, *52*(7), 1397–1403.

Jack, C. R. Jr., Shiung, M. M., Weigand, S. D., O'Brien, P. C., Gunter, J. L., Boeve, B. F., et al. (2005). Brain atrophy rates predict subsequent clinical conversion in normal elderly and amnestic MCI. *Neurology*, *65*(8), 1227–1231. doi:10.1212/01.wnl.0000180958.22678.91.

Jiang, J., Zhu, W., Shi, F., Zhang, Y., Lin, L., & Jiang, T. (2008). A robust and accurate algorithm for estimating the complexity of the cortical surface. *Journal of Neuroscience Methods*, *172*(1), 122–130. doi:10.1016/j.jneumeth.2008.04.018.

Joshi, S., Davis, B., Jomier, M., & Gerig, G. (2004). Unbiased diffeomorphic atlas construction for computational anatomy. *NeuroImage*, *23*(Suppl 1), S151–S160. doi:10.1016/j.neuroimage.2004.07.068.

Killiany, R. J., Gomez-Isla, T., Moss, M., Kikinis, R., Sandor, T., Jolesz, F., et al. (2000). Use of structural magnetic resonance imaging to predict who will get Alzheimer's disease. *Annals of Neurology*, *47*(4), 430–439. doi:10.1002/1531-8249(200004)47:4<430::AID-ANA5>3.0.CO;2-I.

Kiselev, V. G., Hahn, K. R., & Auer, D. P. (2003). Is the brain cortex a fractal? *NeuroImage*, *20*(3), 1765–1774. doi:10.1016/S1053-8119(03)00380-X.

Korf, E. S., Wahlund, L. O., Visser, P. J., & Scheltens, P. (2004). Medial temporal lobe atrophy on MRI predicts dementia in

patients with mild cognitive impairment. *Neurology*, *63*(1), 94–100.

Lee, J. M., Yoon, U., Kim, J. J., Kim, I. Y., Lee, D. S., Kwon, J. S., et al. (2004). Analysis of the hemispheric asymmetry using fractal dimension of a skeletonized cerebral surface. *IEEE Transactions on Bio-Medical Engineering*, *51*(8), 1494–1498. doi:10.1109/TBME.2004.831543.

Liu, J. Z., Zhang, L. D., & Yue, G. H. (2003). Fractal dimension in human cerebellum measured by magnetic resonance imaging. *Biophysical Journal*, *85*(6), 4041–4046.

Majumdar, S., & Prasad, R. R. (1988). The fractal dimension of cerebral surfaces using magnetic resonance imaging. *Computers in Physics*, *2*(6), 69–73.

Mandelbrot, B. B. (1977). *Fractals: Form, chance, and dimension*. San Francisco: W. H. Freeman.

Mandelbrot, B. B. (1982). *The fractal geometry of nature*. San Francisco: W.H. Freeman.

Moorhead, T. W., Harris, J. M., Stanfield, A. C., Job, D. E., Best, J. J., Johnstone, E. C., et al. (2006). Automated computation of the Gyrification Index in prefrontal lobes: Methods and comparison with manual implementation. *NeuroImage*, *31*(4), 1560–1566. doi:10.1016/j.neuroimage.2006.02.025.

Morris, J. C. (1997). Clinical dementia rating: A reliable and valid diagnostic and staging measure for dementia of the Alzheimer type. *International Psychogeriatrics*, *9*(Suppl 1), 173–176, discussion 177–178. doi:10.1017/S1041610297004870.

Mueller, S. G., Weiner, M. W., Thal, L. J., Petersen, R. C., Jack, C., Jagust, W., et al. (2005). The Alzheimer's disease neuroimaging initiative. *Neuroimaging Clinics of North America*, *15*(4), 869–877, xi–xii. doi:10.1016/j.nic.2005.09.008.

Rademacher, J., Caviness, V. S. Jr., Steinmetz, H., & Galaburda, A. M. (1993). Topographical variation of the human primary cortices: Implications for neuroimaging, brain mapping, and neurobiology. *Cerebral Cortex (New York, N.Y.)*, *3*(4), 313–329. doi:10.1093/cercor/3.4.313.

Salamon, N., Sicotte, N., Mongkolwat, P., Shattuck, D., & Salamon, G. (2005). The human cerebral cortex on MRI: Value of the coronal plane. *Surgical and Radiologic Anatomy*, *27*(5), 431–443. doi:10.1007/s00276-005-0022-7.

Smith, T. G. Jr., Marks, W. B., Lange, G. D., Sheriff, W. H. Jr., & Neale, E. A. (1989). A fractal analysis of cell images. *Journal of Neuroscience Methods*, *27*(2), 173–180. doi:10.1016/0165-0270(89)90100-3.

Takayasu, H. (1990). *Fractals in the physical sciences*. Manchester, NY: Manchester University Press, Distributed exclusively in the USA and Canada by St. Martin's Press.

Thompson, P. M., Moussai, J., Zohoori, S., Goldkorn, A., Khan, A. A., Mega, M. S., et al. (1998). Cortical variability and asymmetry in normal aging and Alzheimer's disease. *Cerebral Cortex (New York, N.Y.)*, *8*(6), 492–509. doi:10.1093/cercor/8.6.492.

Thompson, P. M., Mega, M. S., Woods, R. P., Zoumalan, C. I., Lindshield, C. J., Blanton, R. E., et al. (2001). Cortical change in Alzheimer's disease detected with a disease-specific population-based brain atlas. *Cerebral Cortex (New York, N.Y.)*, *11*(1), 1–16. doi:10.1093/cercor/11.1.1.

Thompson, P. M., Hayashi, K. M., Dutton, R. A., Chiang, M. C., Leow, A. D., Sowell, E. R., et al. (2007). Tracking Alzheimer's disease. *Annals of the New York Academy of Sciences*, *1097*, 183–214. doi:10.1196/annals.1379.017.

Toga, A. W., & Thompson, P. M. (2002). New approaches in brain morphometry. *The American Journal of Geriatric Psychiatry*, *10*(1), 13–23. doi:10.1176/appi.ajgp.10.1.13.

Visser, P. J., Scheltens, P., Verhey, F. R., Schmand, B., Launer, L. J., Jolles, J., et al. (1999). Medial temporal lobe atrophy and memory dysfunction as predictors for dementia in subjects with mild cognitive impairment. *Journal of Neurology*, *246*(6), 477–485. doi:10.1007/s004150050387.

Walhovd, K. B., Fjell, A. M., Reinvang, I., Lundervold, A., Dale, A. M., Quinn, B. T., et al. (2005). Neuroanatomical aging: Universal but not uniform. *Neurobiology of Aging*, *26*(9), 1279–1282. doi:10.1016/j.neurobiolaging.2005.05.018.

Wang, L., Swank, J. S., Glick, I. E., Gado, M. H., Miller, M. I., Morris, J. C., et al. (2003). Changes in hippocampal volume and shape across time distinguish dementia of the Alzheimer type from healthy aging. *NeuroImage*, *20*(2), 667–682. doi:10.1016/S1053-8119(03)00361-6.

Yu, P., Grant, P. E., Qi, Y., Han, X., Segonne, F., Pienaar, R., et al. (2007). Cortical surface shape analysis based on spherical wavelets. *IEEE Transactions on Medical Imaging*, *26*(4), 582–597. doi:10.1109/TMI.2007.892499.

Zhang, L., Liu, J. Z., Dean, D., Sahgal, V., & Yue, G. H. (2006). A three-dimensional fractal analysis method for quantifying white matter structure in human brain. *Journal of Neuroscience Methods*, *150*(2), 242–253. doi:10.1016/j.jneumeth.2005.06.021.

Zhang, L., Dean, D., Liu, J. Z., Sahgal, V., Wang, X., & Yue, G. H. (2007). Quantifying degeneration of white matter in normal aging using fractal dimension. *Neurobiology of Aging*, *28*, 1543–1555.

Zilles, K., Armstrong, E., Schleicher, A., & Kretschmann, H. J. (1988). The human pattern of gyrification in the cerebral cortex. *Anatomy and Embryology*, *179*(2), 173–179. doi:10.1007/BF00304699.

Zilles, K., Armstrong, E., Moser, K. H., Schleicher, A., & Stephan, H. (1989). Gyrification in the cerebral cortex of primates. *Brain, Behavior and Evolution*, *34*(3), 143–150. doi:10.1159/000116500.